ACS APPLIED ELECTRONIC MATERIALS

pubs.acs.org/acsaelm Article

Empowering Bioelectronics with Supramolecular Nanoarchitectonics: PEDOT-Based Organic Electrochemical Transistors with Tunable Electronic Properties

Joaquin F. Diforti, Esteban Piccinini,* Juan A. Allegretto, Catalina von Bilderling, Waldemar A. Marmisollé,* and Omar Azzaroni

Cite This: *ACS Appl. Electron. Mater.* 2024, 6, 1211−1222 Read Online

ACCESS | Metrics & More | Article Recommendations | Supporting Information

ABSTRACT: Organic bioelectronics has the potential to unlock the utmost innovation in medicine and healthcare through the combination of biological and digital realms. Particularly, organic electrochemical transistors (OECTs) are a promising class of bioelectronics transducer. Nevertheless, a fabrication strategy is needed to lower the access barrier to the OECTs, thereby expediting product development and innovation. In this work, we present a supramolecular approach with simple equipment to prepare conductive films based on poly(3,4-ethylenedioxythiophene):poly(styrenesulfonate), PEDOT:PSS, integrated with cationic molecular blocks for OECTs manufacturing. By employing the layer-by-layer (LbL) self-assembly technique, we facilely prepared transistor channels of PEDOT:PSS integrated with either the surfactant cetyltrimethylammonium bromide, CTAB, or the polyelectrolyte poly(diallyldimethylammonium chloride), PDADMAC, with nanometric precision. Both cationic blocks feature positively charged quaternary amines but possess different mesogenic and surfactant features. The PEDOT:PSS/CTAB system yields an electrical conductivity of 275 S m^{-1}, which is 4 orders of magnitude higher than those integrated with PDADMAC (0.0531 S m^{-1}). This enhancement is attributed to CTAB integration, which boosts the PEDOT:PSS charge transport, while PDADMAC diminishes it. The electronic performance indicators of OECTs (current at the on-state, I_{max}, threshold potential, V_{TH}, transconductance, g_m) are easily tuned by adjusting the thickness of the transistor channel film. The cycling stability of the transistor channel is 8-fold enhanced by coating it with a protective layer using nonelectroactive polymers. These OECTs exhibit a g_m of 2.21 mS, a μC^* product (μ is the hole mobility, and C^* is the capacitance per unit of volume) of 0.23 F cm^{-1} V^{-1} s^{-1}, and on- and off-switching times, τ, of 24.2 and 12.3 ms, respectively. Their performance was comparable to or better than OECTs with channels prepared using techniques based on equipment of higher complexity and cost. Finally, we demonstrate the utility of these facilely prepared OECTs in biosensing the neurotransmitter dopamine with an exceptional sensitivity of 279 mV/decade and good operation range (1−300 μM) and reversibility.

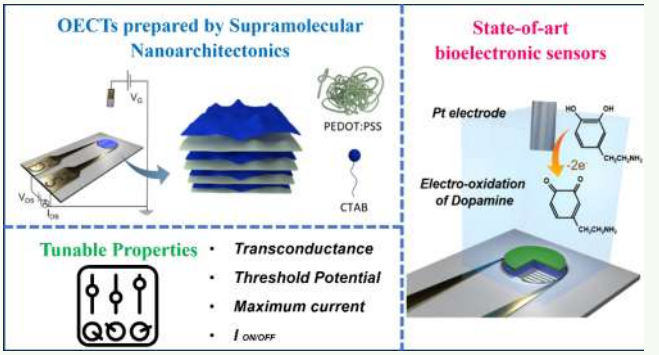

KEYWORDS: *organic electrochemical transistors, PEDOT, bioelectronics, layer-by-layer assembly, dopamine*

INTRODUCTION

During the past decade, mankind has achieved a rapid development in biotechnology and electronics, whose convergence can generate unique advances in different areas.[1−3] However, the union of these fields has not yet reached all the hoped-for impact due to the difficulty of interfacing the biological and digital world.[4] In this context, organic bioelectronics combines organic materials with biology and electronics. Because conducting organic polymers present a unique combination of both electronic and ionic conductivity, these materials are excellent tools to effectively interface biology with digitalized electronics.[4,5] In particular, organic electrochemical transistors (OECTs) have emerged as a promising class for bioelectronic applications because of their distinctive properties such as high interfacial sensitivity, efficient transport, and coupling of ionic and electronic charge, and can be scaled-up in flexible and miniaturized formats.[6−8] These devices consist of an organic semiconductor film that connects source and drain electrodes and whose conductivity can be regulated by the application of a gate voltage (V_G) through an electrolyte.[9,10]

Received: November 11, 2023
Revised: January 22, 2024
Accepted: January 23, 2024
Published: February 7, 2024

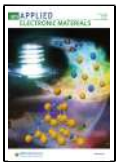

https://doi.org/10.1021/acsaelm.3c01592
ACS Appl. Electron. Mater. 2024, 6, 1211−1222

Poly(3,4-ethylenedioxythiophene) (PEDOT) is a conducting polymer that exhibits high conductivity over a wide potential range, excellent stability in biological environments, and biocompatibility.[11,12] Furthermore, integrating other components such as polystyrenesulfonate and polyallylamine into the PEDOT polymer matrix can result in hybrid compounds (ionic polymer complexes) with new or optimized properties.[13,14] These qualities make PEDOT one of the most attractive conducting polymers for the fabrication of a wide range of (bio)electronic devices. The fabrication of OECTs for bioelectronic applications requires the preparation of thin films of PEDOT with controlled thickness and specific geometric configurations.[15] Techniques such as photolithography, printed circuit board and 3D polymer printers, spin coating, and electrochemical polymerization are commonly employed to construct these films.[16,17] Although the techniques themselves are not complex, the requirement for specific equipment (e.g., lithography equipment, modern printers, etc.) poses a barrier to the preparation of such devices in biology, biotechnology, and data science laboratories. Therefore, there is a need for a strategy that helps lower the access barrier to the fabrication of conducting channels for OECTs with controlled properties to accelerate the development of innovative products that interface biotechnology and digital technologies.

In this context, the use of nanoarchitectonics strategies,[18,19] such as the layer-by-layer (LbL) assembly, is a very attractive and well-constituted technique that allows the nanoconstruction of films with nanometric precision in a simple and scalable way.[19−23] The technique consists of the surface adsorption of components with attractive interactions, such as the electrostatic interaction between blocks of opposite charge. In terms of the relationship between nanoconstruction precision and technical simplicity, this strategy is without a doubt one of the best. Although the LbL technique has been widely used for the construction of different functional interfaces, it has been little explored for the preparation of PEDOT films with integrated components that constitute the active channel of OECTs devices. While certain studies have delved into enhancing the functionality of the pre-existing PEDOT-based conducting channel through the application of a coating via LbL assembly of insulating polyelectrolytes for various purposes,[24−26] the potential benefits of the LbL method for precisely incorporating the PEDOT building block and thereby augmenting the thickness of the conducting channel have been relatively underexplored. In this regard, Zhu et al. have recently reported the LbL preparation of PEDOT-based conducting channels on cotton fibers using PEDOT:PSS and poly(diallyldimethylammonium chloride) (PDADMAC) as counter polyelectrolytes for the fabrication of OECTs that allow the detection of sialic acid.[27] However, in that fiber-based organic electrochemical transistor (FECT) the LbL assembly was used to build conducting fibers, and no studies on the step-by-step addition of conducting material were reported. Despite the recent discoveries, we are far from having harnessed the power of LbL to accelerate the design and development of new materials for the active channels in the OECTs by exploiting the fact that a controllable addition of conducting material can be integrated to produce the conducting channel, and intimate contact between the counterparts can be easily achieved.

In this work, we demonstrate that the construction of conducting channels for OECTs using the anionic electroactive complex poly(3,4-ethylenedioxythiophene):poly(styrenesulfonate), PEDOT:PSS (where PEDOT is doped with the anionic agent PSS),[28] can be achieved in a very simple manner using the LbL technique. The application of this supramolecular technique in nanoconstructing the conductive channel allows for the incorporation of three readily adjustable design variables: (i) the selection of building blocks to confer specific features to the resulting OECT channel (in addition, multiple components can be used for leading to multifunctional films); (ii) the number of assembly cycles for controlling the quantity of deposited material; and (iii) the nanoarchitectonic order of the assembled components to trigger complementary properties. Here, we illustrate how the proper combination of building blocks is decisive for producing functional conducting channels for bioelectronic applications. Furthermore, we show that this technique allows the fine-tuning of the electronic properties of the transistors by adjusting their channel thickness. In this regard, we comparatively investigated two combinations: PEDOT:PSS assembled with the polyelectrolyte PDADMAC and PEDOT:PSS assembled with the surfactant cetyltrimethylammonium bromide (CTAB). Both cationic blocks are electrochemically inactive and have positive charge consisting of quaternary amines but with different mesogenic and surfactant characters, which may lead to different structure.[29,30] On the one side, the mesogenic character is the property of some compounds to promote molecular order or spatial orientation of the structures generated in combination with other reagents such as polymers.[31] For instance, it has been shown that the presence of surfactants in LbL assemblies has a strong impact on structure−property relationship composite.[30,32,33] On the other hand, the surfactant character may disperse building blocks and enhance the interchain interactions between conducting polymer.[34] In this sense, the integration of CTAB into the LbL structure may promote structural changes with implications on the electronic conductivity of the films compared with the long chain polyelectrolyte PDADMAC. For both systems, we studied the growth, thickness, and surface topography of the films and the doping state of PEDOT using UV−vis spectrophotometry, spectroscopic ellipsometry, atomic force microscopy (AFM), and Raman spectroscopy, respectively. Moreover, charge transport was evaluated as a function of the number of bilayers by studying the electrical resistance and field-effect transistor behavior. From transfer and transient characteristics of the transistors, key performance indicators such as current at the on-state (I_{max}), I_{on}/I_{off} ratio, threshold potential (V_{TH}), transconductance (g_m), and on- or off-switching time were obtained as a function of the number of bilayers. The stability of the transistors was improved by an external nonelectroactive layer that acts as a protective layer, also prepared using LbL. Finally, we demonstrated how these easily prepared OECTs can be used for biosensing of the neurotransmitter dopamine with great sensitivity, without any extra modification of the electrodes and in a very simple electrolytic medium.

MATERIALS AND METHODS

Reagents and Materials. Absolute ethanol, (3-aminopropyl)-triethoxysilane (APTES) (>98%), poly(3,4-ethylenedioxythiophene):polystyrenesulfonate (PEDOT:PSS) 0.5−1.0% in H_2O, poly(diallyldimethylammonium chloride) (PDADMAC) 20% in H_2O (average $M_W \sim 100000-200000$), cetyltrimethylammonium bromide (CTAB) (>99%), and poly(4-styrenesulfonate) sodium (PSS) (average $M_W \sim 1000000$) were obtained from Sigma-Aldrich. KCl was purchased from Biopack (>99%), NaCl was purchased from Merck (99.5%), ammonium hydroxide (28.3% in H_2O) was obtained

https://doi.org/10.1021/acsaelm.3c01592
ACS Appl. Electron. Mater. 2024, 6, 1211−1222

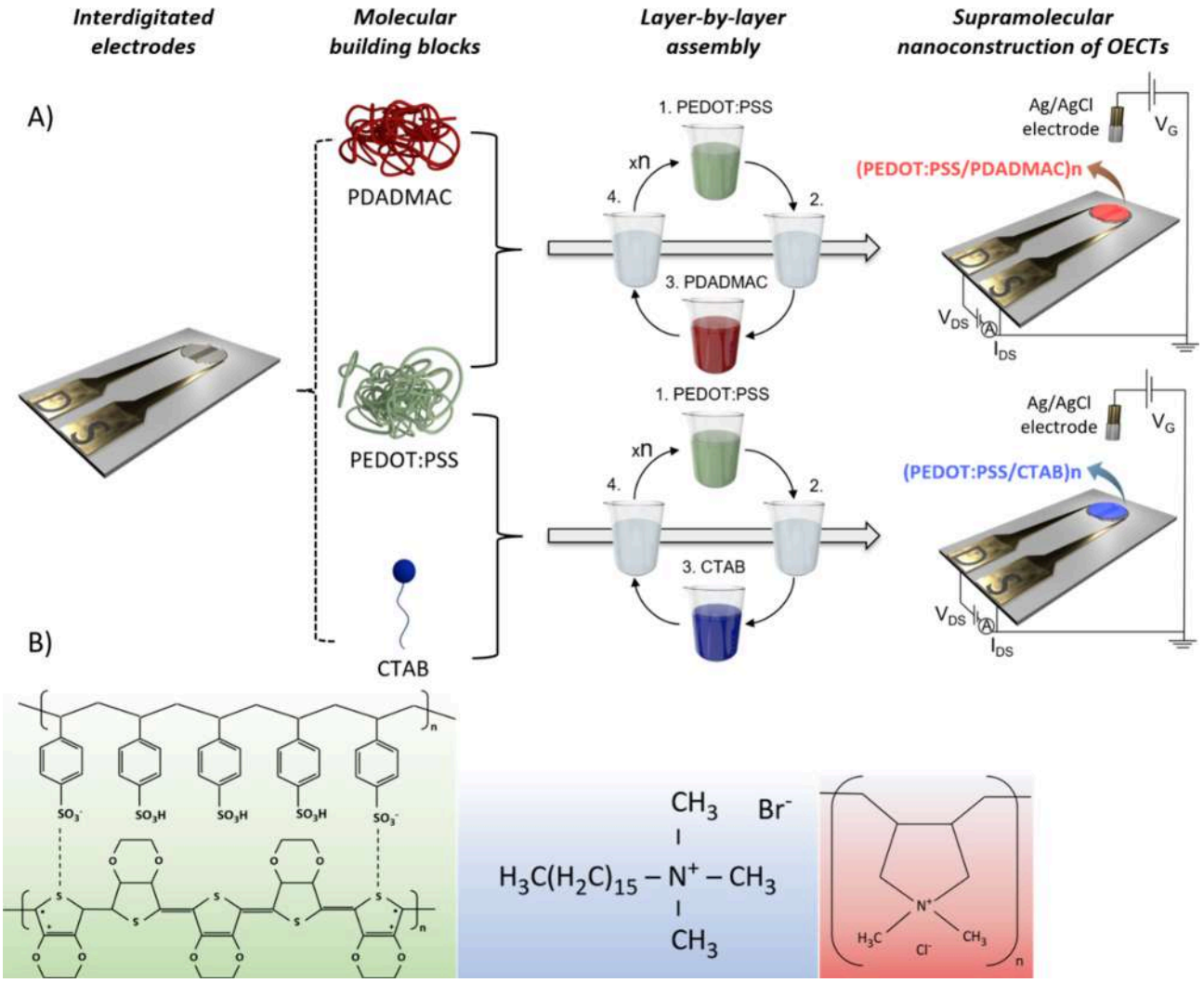

Figure 1. (A) Schematic representation of the LbL nanoconstruction of the conducting assemblies for the manufacturing of (PEDOT:PSS/PDADMAC)$_n$ (top) and (PEDOT:PSS/CTAB)$_n$ (bottom) OECTs. (B) Molecular structure of the PEDOT:PSS complex (green), surfactant CTAB (blue), and polycation PDADMAC (red).

from Cicarelli, and hydrogen peroxide was from Chemical Specialties. NaCl and KCl solutions were prepared with Milli-Q water. All the polyelectrolyte (1 mg/mL) and surfactant (2 mM CTAB) solutions were prepared in 0.1 M NaCl to keep a constant ionic strength and sonicated for 10 min. The 2 mM CTAB solution is over the critical micelle concentration (CMC = 0.98 mM at 25 °C). Interdigitated electrodes (ED-IDE1-Au, 10/10 μm electrode/gap) were obtained from Micrux Technologies (Spain). Monocrystalline (100) Si wafers were used for surface topography and spectroscopic ellipsometry studies.

OECT Fabrication. The preparation of OECTs was adapted from previously reported protocols.[35] In the first step, commercial glass substrates containing interdigitated gold electrodes with 10/10 μm electrode/gap were cleaned with a NH_4OH:H_2O_2:H_2O solution (1:1:5) at 60 °C for 25 min, rinsed with Milli-Q water, and dried. Second, the substrates were functionalized with 2% APTES in EtOH for 1 h, followed by 2 h thermal annealing at 120 °C. Finally, the organic channel of the transistor was prepared by the LbL nanoconstruction technique of PEDOT:PSS and the cationic molecular blocks. Thus, the drain and source terminals of the OECTs are gold interdigitated electrodes, and the gate is an Ag/AgCl pseudoreference electrode. The gate electrode is connected to the transistor channel by an electrolytic solution; this configuration is known as electrolyte-gated transistor.

The LbL assembly process was started by making use of protonated amino groups from APTES as positive anchoring groups. The construction of each bilayer consisted of soaking the substrates, successively and alternatively, in the anionic building block solution (1 mg/mL PEDOT:PSS in 0.1 M NaCl) for 10 min, rinsing with deionized water for 5 min, and then soaking in the corresponding cationic building block solution (2 mM CTAB or 1 mg/mL PDADMAC, both in 0.1 M NaCl) for 10 min and rinsing with deionized water. All the solutions contained 0.1 M NaCl to favor the polymer deposition.[36] The previous processes were repeated until the desired number of bilayers. In this way, (PEDOT:PSS/PDADMAC)$_n$ and (PEDOT:PSS/CTAB)$_n$ assemblies as organic channel of the transistors of different number of bilayers (n) were constructed. Furthermore, in order to improve the structural stability of the (PEDOT:PSS/CTAB)$_n$ conducting channels, they were covered with a nonelectroactive (PSS/PDADMAC)$_3$ assembly. The OECTs were incubated, successively and alternatively, in 1 mg/mL PSS for 10 min and then in 1 mg/mL PDADMAC for 10 min. Washing between each layer deposition was done by submerging the assembly into deionized water for 5 min in quiescent conditions. Thus, (PEDOT:PSS/CTAB)$_n$(PSS/PDADMAC)$_3$ films were obtained.

UV−Visible Spectrophotometry. The film growth was studied employing a UV−vis HP 8453E spectrophotometer in a spectral range between 400 and 1000 nm. The dispersion on the absorbance value of the assemblies was set as the standard deviation (SD) of 3 replicates.

https://doi.org/10.1021/acsaelm.3c01592
ACS Appl. Electron. Mater. 2024, 6, 1211−1222

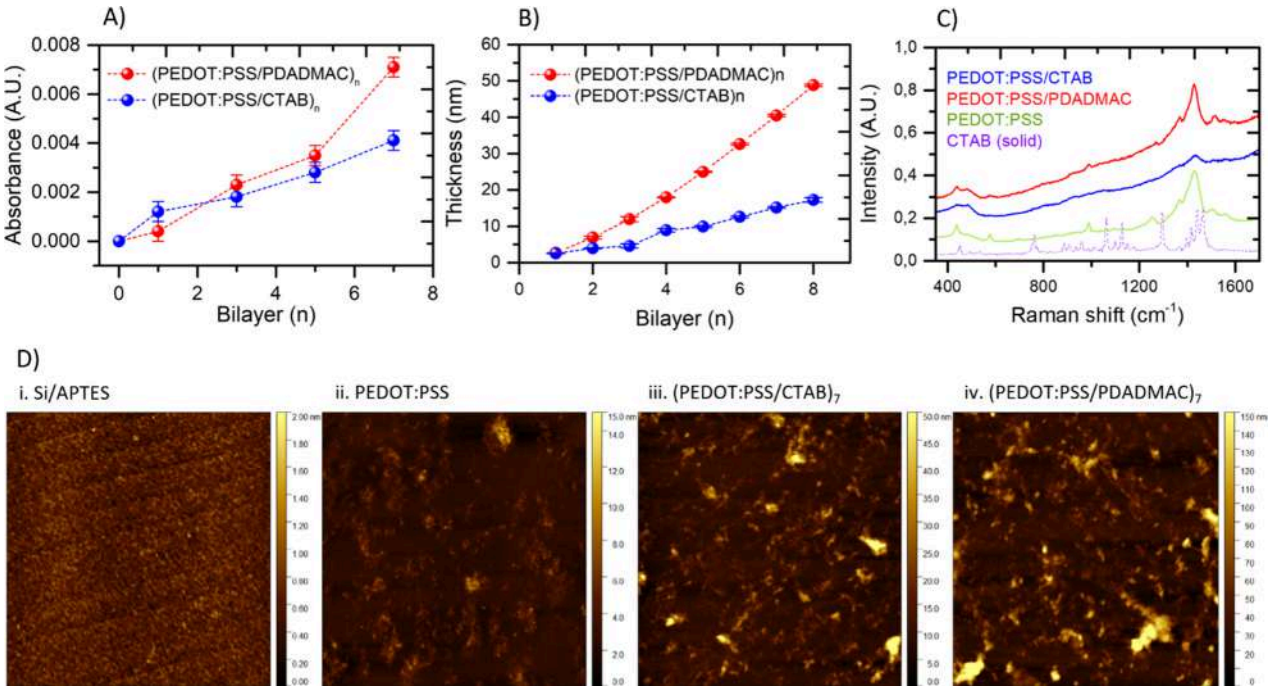

Figure 2. (A) Absorbance at 955 nm of (PEDOT:PSS/PDADMAC)n (red) and (PEDOT:PSS/CTAB)n (blue) films as a function of the number of bilayers (n) assembled. The shown values are the average of three replicate devices, and the error bar corresponds to the standard deviation (SD). (B) Film thickness obtained by ellipsometry of $(PEDOT:PSS/PDADMAC)_n$ (red) and $(PEDOT:PSS/CTAB)_n$ (blue) assemblies as a function of n. The error bar corresponds to the SD of three measurements on different areas of the same device. Solid lines are just eye guides. (C) Raman spectra of PEDOT:PSS (green), PEDOT:PSS/CTAB (blue), and PEDOT:PSS/PDADMAC (red) films and CTAB solid sample (purple). (D) AFM images (10 × 10 μm^2) of (i) Si/APTES substrate, (ii) a PEDOT:PSS layer, (iii) $(PEDOT:PSS/CTAB)_7$, and (iv) $(PEDOT:PSS/PDADMAC)_7$ films.

Raman Spectrophotometry. Raman studies were performed using an i-Raman BW415-532S (BWTek) Raman spectrometer with an excitation wavelength of 532 nm. The laser was focused on the substrates by a 20× optical microscope (BAC151B, BWTek).

Surface Topography and Film Thickness. The topographic properties of the assemblies were evaluated, at each stage of their construction, by AFM (Keysigth 5500 SPM), and the root-mean-square (RMS) roughness was determined. AFM measurements were performed in AC mode in air using Tap190Al-G probes (Budget-Sensors). Both the analysis and the processing of the images obtained were performed by using Gwyddion software.

The thickness and optical properties of the films and LbL assemblies were analyzed by spectroscopic ellipsometry (180 wavelengths from 380 to 900 nm) in an Alpha-SE apparatus from J. A. Woollam. All measurements were done at 70° incidence with high precision alignment routines and a long acquisition time. Both PEDOT:PSS/cationic block and (PSS/PDADMAC) assemblies were modeled as Cauchy layers unless stated otherwise (see the Supporting Information for further details).

Electrical Resistance and Field-Effect Measurements. The electrical resistance between the interdigitated electrodes (i.e., the OECT channel) was measured with an Agilent Technologies U1241A multimeter after each bilayer was prepared. The dispersion was calculated for every experimental arrangement as the SD of 3 replicates (independent sensors) of each assembly condition.

To study the field-effect properties of the OECTs, transfer characteristics curves (I_{DS}–V_G) and transient curves (I_{DS}–t) were acquired. Both transfer and transient characteristics were obtained by employing a TEQ-04 bipotentiostat (Nanoteq, Argentina). To achieve the electrolyte-gated transistor configuration, a 3D printed electrochemical cell was used (see Figure 4A). It allowed D–S terminals connection, the gate fixing, and the physical contact between the electrolytic solution with the assembly and the gate terminal, as reported elsewhere.[35,37] All the measurements were performed in 0.1 M KCl electrolytic solution and employing a Ag/AgCl (pseudoreference) electrode gate. For transfer measurements a variable gate potential between −350 and 800 mV was applied (using a constant drain–source potential of 50 mV), at a sweep rate of 10 mV s^{-1}, unless otherwise stated. For transient measurements, a square pulse potential was applied, composed of a stable potential of 700 mV and periodic pulses of −350 mV, every 3 s.

RESULTS AND DISCUSSION

Film Nanoconstruction, Chemical Characterization, Water Content, and Surface Topography. Conductive thin films were prepared using the layer-by-layer (LbL) nanoconstruction technique between the anionic electroactive complex PEDOT:PSS, and the cationic molecular blocks PDADMAC (polyelectrolyte) or CTAB (surfactant) (Figure 1A). Thus, the systems built were $(PEDOT:PSS/PDADMAC)_n$ and $(PEDOT:PSS/CTAB)_n$ where n corresponds to the number of bilayers. The growth and thickness of the films as a function of n were studied by UV–vis spectrophotometry[38] and spectroscopic ellipsometry.[39] The assemblies were prepared on glass and silicon substrates previously modified with 3-(aminopropyl)triethoxysilane (APTES). APTES functionalizes the surface of the substrate with amino groups, which are protonated at the working pH, giving the surface a positive charge. Then, the LbL assembly was performed by the alternated incubation of the substrate in 1 mg/mL PEDOT:PSS (anionic block, Figure 1B) and 1 mg/mL PDADMAC or CTAB (cationic blocks, Figure 1B), washing with deionized between steps.

For PEDOT:PSS and PDADMAC solutions, the concentration values were obtained from a previously optimized protocol.[36] To define the CTAB optimal concentration, the effect of the concentration on the growth of the assembly of

https://doi.org/10.1021/acsaelm.3c01592
ACS Appl. Electron. Mater. 2024, 6, 1211–1222

$(PEDOT:PSS/CTAB)_7$ was studied by measuring the absorbance of the film. Four different concentrations were used: two concentrations below the critical micelle concentration (CMC = 0.98 mM at 25 °C)[40] and two above the CMC. The concentrations tested were 0.05, 0.10, 2.00, and 4.00 mM. To monitor the different assemblies by UV−vis absorbance, the wavelength of maximum absorbance of PEDOT:PSS (955 nm; see Figure S1 for more details) was used. Among the 4 systems tested, that corresponding to a concentration of 2 mM was the one that presented the highest absorbance value, while that of 4 mM presented the lowest value (Figure S2). This decrease in absorbance value could be due to a partial desorption of the PEDOT:PSS deposited layer from the assembled film caused by an excess of surfactant (concentration well above CMC). Based on these results, the concentration selected to continue with the proposed study was 2 mM CTAB. Figure 2A shows the absorbance of the LbL assemblies prepared by using both cationic blocks. An approximately linear growth was obtained for $(PEDOT:PSS/CTAB)_n$, while a supralinear behavior is obtained for $(PEDOT:PSS/PDADMAC)_n$. Linear film growth behavior was described to be typically displayed for LbL assemblies with component adsorption governed by intrinsic neutralization.[41] The supralinear growing up of LbL films containing PEDOT:PSS and cationic polyelectrolytes has been previously described.[42,43] This behavior has been also well described and characterized for the assembly of PSS and PDADMAC,[44] which has been assigned to the fact that during PDADMAC adsorption, part of the chains adsorb directly onto the previous PSS layer through an intrinsic charge compensation mechanism and part of the chains form tails or loops into the solution, increasing the roughness of the coating.[41]

Thickness progression for the assembly of the conductive film was tracked by spectroscopic ellipsometry (Figure S4). In line with UV−vis spectroscopy results, the use of CTAB as counterpart for the PEDOT:PSS block leads to a linear growth regime, while the use of PDADMAC develops a supralinear growth (Figure 2B), which is associated with a rough surface, as confirmed by AFM measurements (vide infra). Although the first bilayer has roughly the same thickness (2.5 ± 0.1 and 2.7 ± 0.1 nm for CTAB and PDADMAC systems, respectively), by the fifth bilayer the thickness for PDADMAC-based assemblies (25.0 ± 0.2 nm) is almost 2.5 times higher than for CTAB-based assemblies (9.9 ± 0.3 nm), and this difference even increases as the number of layers further increases. Another interesting comparison between both assemblies is that despite the thickness differences, the polymer volume fraction of the films (n = 7) is the same. By using the Bruggeman approximation to effective medium theory (see the Supporting Information) and comparing the assemblies in dry and wet states (i.e., by using a flow cell and exposing the assembly to water), we have found a water uptake of 40% of the film volume for both assemblies. This result suggests that despite the thickness differences, both assemblies are equally accessible to the solvent in *in operando* conditions.

The Raman spectrum for a PEDOT:PSS layer (prepared by drop casting) presents peaks with a very good correlation with the literature (green line in Figure 2C). For instance, the 438 cm^{-1} peak is assigned to SO_2 bending, 577 cm^{-1} is related to oxyethylene ring deformation, 1255 cm^{-1} is the $C_\alpha-C_\alpha$ inter-ring stretching, 1365 cm^{-1} to $C_\beta-C_\beta$ stretching, 1431 cm^{-1} to symmetric $C_\alpha{=}C_\beta(-O)$ stretching, and the 1510/1563 cm^{-1} peak is assigned to the asymmetric $C_\alpha{=}C_\beta$ stretching.[45,46] As expected from the resonant effect in PEDOT block which strongly absorb at 532 nm (see Figure S1), the PEDOT:PSS contribution dominates the spectra of the composites with cationic blocks (these blocks do not absorb at 532 nm). Thus, the PEDOT:PSS/cation block assemblies (blue and red lines in Figure 2C) showed the presence of all the peaks assigned to PEDOT:PSS. However, the characteristic peak of CTAB at 1061 cm^{-1}[47] is also presented in the PEDOT:PSS/CTAB film spectrum, confirming the presence of this block.

The surface topography was studied by using AFM. Micrographs were obtained for samples before and after the LbL assemblies (Figure 2D). The root-mean-square (RMS) roughness was calculated from each image (Table 1). It is noted that films of n = 7 prepared with CTAB display significantly less roughness (higher uniformity) than those prepared with PDADMAC. The roughness difference between both systems may be due to their different mesogenic and surfactant properties.

Table 1. RMS Roughness Estimated from the AFM Micrographs Obtained for the Different Assemblies[a]

sample	RMS roughness (nm)
Si/APTES	0.15 ± 0.01
Si/APTES/PEDOT:PSS	1.0 ± 0.1
$Si/APTES/(PEDOT:PSS/PDADMAC)_1$	1.6 ± 0.2
$Si/APTES/(PEDOT:PSS/CTAB)_1$	2.3 ± 0.5
$Si/APTES/(PEDOT:PSS/PDADMAC)_7$	19 ± 6
$Si/APTES/(PEDOT:PSS/CTAB)_7$	5 ± 1

[a]The error corresponds to the SD of five measurements on different areas (of 5 × 5 μM) for each system.

Electrical Resistance and the Effect of CTAB as Charge Transport Enhancer. After the growth and topography of the assemblies were studied, the electronic resistance (R) of the conducting films was evaluated. For this, the conducting assemblies were prepared on glass substrates containing interdigitated gold electrodes (Figure 3A), and the electrical resistance was measured between the electrode contacts (drain−source resistance). Figure 3B shows the electrical resistance as a function of n for both systems: $(PEDOT:PSS/PDADMAC)_n$ and $(PEDOT:PSS/CTAB)_n$. The electrical resistance decreases exponentially with film growth, which is equivalent to an increase in the conductance. It is important to highlight that the system containing CTAB as a cationic molecular building block yields films with a conductance 3 orders of magnitude higher than the system with PDADMAC.

By measuring the conductivity of the film after each layer is assembled, it is possible to address the contribution of each cationic molecular block (Figure 3C). After the deposition of PDADMAC on PEDOT:PSS, the resistance increased by 1 order of magnitude. On the other hand, after the deposition of CTAB on PEDOT:PSS, the resistance decreased by approximately 2 orders of magnitude. Therefore, the integration of the surfactant generates a great improvement in the charge transport of the film, which is a striking result because CTAB is not electroactive. This effect may be due to the mesogenic and surfactant properties of the CTAB that drive the internal organization of the resulting assembly and the dispersion of building block domains that could enhance the interchain interactions between conducting polymer.[34] It is reported in the literature that CTAB in conjunction with polyelectrolytes

https://doi.org/10.1021/acsaelm.3c01592
ACS Appl. Electron. Mater. 2024, 6, 1211−1222

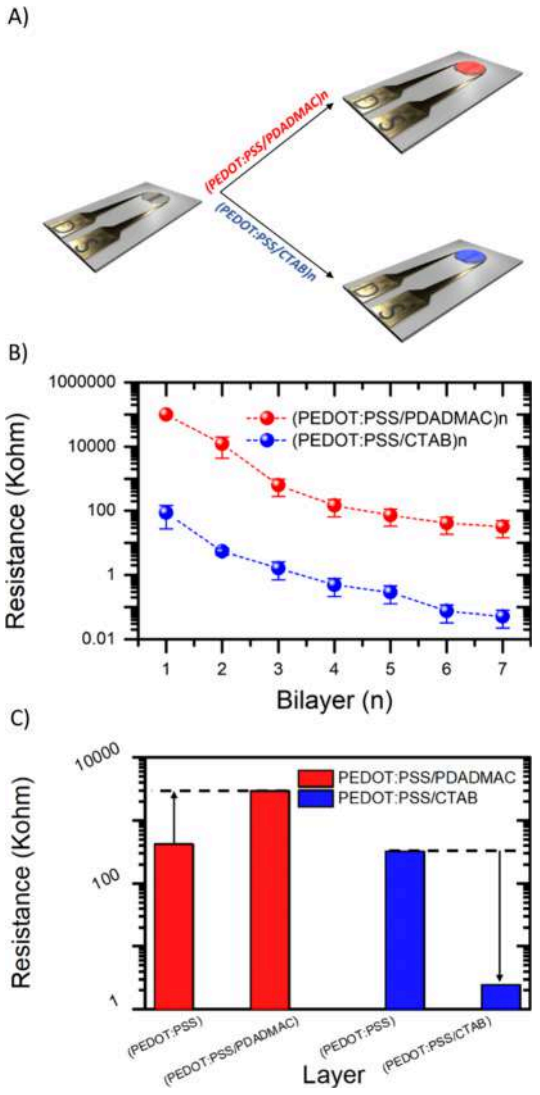

Figure 3. (A) Schematic representation of $(PEDOT:PSS/PDADMAC)_n$ (top) and $(PEDOT:PSS/CTAB)_n$ (bottom) films on the interdigitated electrodes. (B) Electrical resistance between D−S terminals of $(PEDOT:PSS/PDADMAC)_n$ (red) and $(PEDOT:PSS/CTAB)_n$ (blue) assemblies as a function of n. The showed values are the average of three replicate devices, and the error bar corresponds to the standard deviation (SD). (C) Electrical resistance for different deposited layers: PEDOT:PSS, $(PEDOT:PSS/PDADMAC)_1$, and $(PEDOT:PSS/CTAB)_1$.

generates meso-organized structures with a predominantly circular orthogonal phase.[29,40] On the other hand, it has also shown that the LbL of polyelectrolytes and surfactants can yield mesoscopic order with domains aligned parallel to the substrate.[34] When electroactive polymers are used, such structure has been shown to produce electroactive and stable films in aqueous solutions.[48] This alignment of the conducting domains parallel to the substrate is likely to improve the in-plane conductivity. Furthermore, the plasticizing role of surfactants has been also reported to be responsible for the increase of the electronic conductivity in polyaniline (PANI) composites due to the induction of self-organization in the structure of the PANI-based materials.[49,50]

The electrical conductivity (σ) of each assembly system was calculated by using the equation $\sigma = Gx\frac{l}{A}$, where G represents the electrical conductance of the assembly defined as $1/R$, l is the distance that separates the interdigitated electrodes (10 μm), and A the cross-sectional area of the assembly, calculated as the product between the ellipsometric film thickness and the total contour of the interdigitated electrodes (23.5 cm). Values of 0.053 ± 0.029 and 275 ± 160 S/m were obtained for $(PEDOT:PSS/PDADMAC)_7$ and $(PEDOT:PSS/CTAB)_7$, respectively. Thus, conductivity for the PEDOT:PSS/CTAB system was almost 4 orders of magnitude higher. It has been reported that PEDOT-based systems prepared by LbL assemblies such as $(P3HT\text{-}R/PEDOT:PSS)_n$, $(PDADMAC/PEDOT:PSS)_n$, and $(PEDOT\text{-}S/PAH)_n$ display conductivities of 2,[51] 0.1−0.8,[38] and 0.025 S/m,[52] respectively. Therefore, the PEDOT:PSS/CTAB integrated system overcomes many PEDOT-based LbL architectures previously reported.

Charge Transport Study by Field-Effect Measurements and Optimization of the Transistor Electroactivity. The charge transport properties were evaluated by field-effect studies using the $(PEDOT:PSS/cation\ block)_n$ films as a semiconductor channel of organic electrochemical transistors (OECTs, see Figure 4A). To this end, the conducting LbL assemblies were prepared on the substrate with the pair of interdigitated electrodes which worked as the drain and source electrodes of the OECT. A Ag/AgCl pseudoreference electrode was used as the gate electrode (Figure 4A). In these devices, it is possible to study the change in the conductivity of the films as a function of the redox state of the PEDOT:PSS conducting complex. For this purpose, transfer characteristic curves ($I_{DS}-V_G$) are obtained, which show the current that flows through the conductive film (I_{DS}) during application of the variable gate potential (V_G). In OECTs, electronic and ionic charge transport mainly occur in orthogonal directions: the electronic transport through the drain−source electrodes (horizontal) and the ionic transport through the solution/film interface (vertical).[53] The $I_{DS}-V_G$ curves were tested for each type of assembly by using a 0.1 M KCl electrolytic solution. The following charge transport parameters of interest were determined: (i) the maximum I_{DS} value (I_{max}) corresponding to the conductive or oxidized state (on-state), (ii) the I_{on}/I_{off} ratio, (iii) the threshold potential (V_{TH}), and (iv) the transconductance (g_m) (see Figure S5 and the Supporting Information for calculation details).

In order to evaluate the field effect properties as a function of the number of assembled bilayers, films of 3, 5, and 7 bilayers were constructed for the $(PEDOT:PSS/CTAB)_n$ and $(PEDOT:PSS/PDADMAC)_n$ assemblies and measured in OECT configuration (see Figure 4B and Figure S9). The transfer curves of the film $(PEDOT:PSS/CTAB)_n$ show typical electrochemical behavior for depletion mode OECTs. That is, in the absence of applied V_G, the organic semiconductor PEDOT exhibits P-type doping (holes as charge carriers), where PSS stabilizes its oxidized form from its anion sulfonate and presents a high conductivity. In this way, and in our devices, I_{DS} is maximum at negative V_G and begins to decrease exponentially to zero toward increasing V_G value. This effect is due to the reduction of PEDOT, known as "electrochemical dedoping", where the electrolyte cations in solution are injected into the reduced PEDOT:PSS channel to compensate for the charge of the sulfonate anions. This condition leads to the loss of conductivity of the film, and the transistor reaches its off state. In addition, and in accordance with the electrical resistance measurements, an increase in the current of the conducting state (I_{max}) is observed with the increase in the

https://doi.org/10.1021/acsaelm.3c01592
ACS Appl. Electron. Mater. 2024, 6, 1211−1222

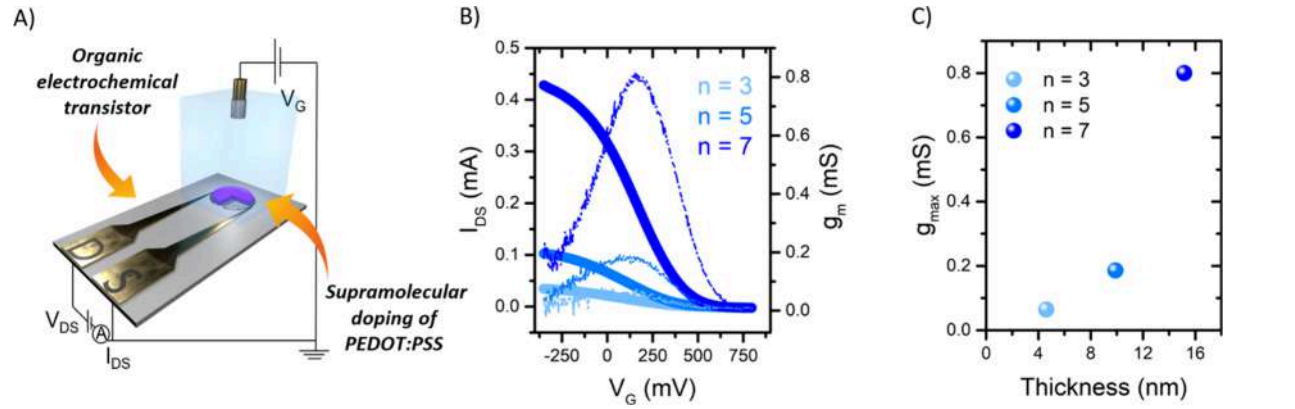

Figure 4. (A) Schematic representation of the $(PEDOT:PSS/cationic\ block)_n$ OECT. (B) Transfer curves (solid line, left-Y) and transconductance curves (dashed line, right-Y) as a function of V_G for $(PEDOT:PSS/CTAB)_n$ OECTs. (C) Values of maximum transconductance (g_{max}) as a function of film thickness for $(PEDOT:PSS/CTAB)_n$ OECTs. Results correspond to films with 3, 5, and 7 bilayers in 0.1 M KCl electrolytic solution, applying a V_G sweep between −350 and 800 mV at 10 mV/s and a V_{DS} of 50 mV.

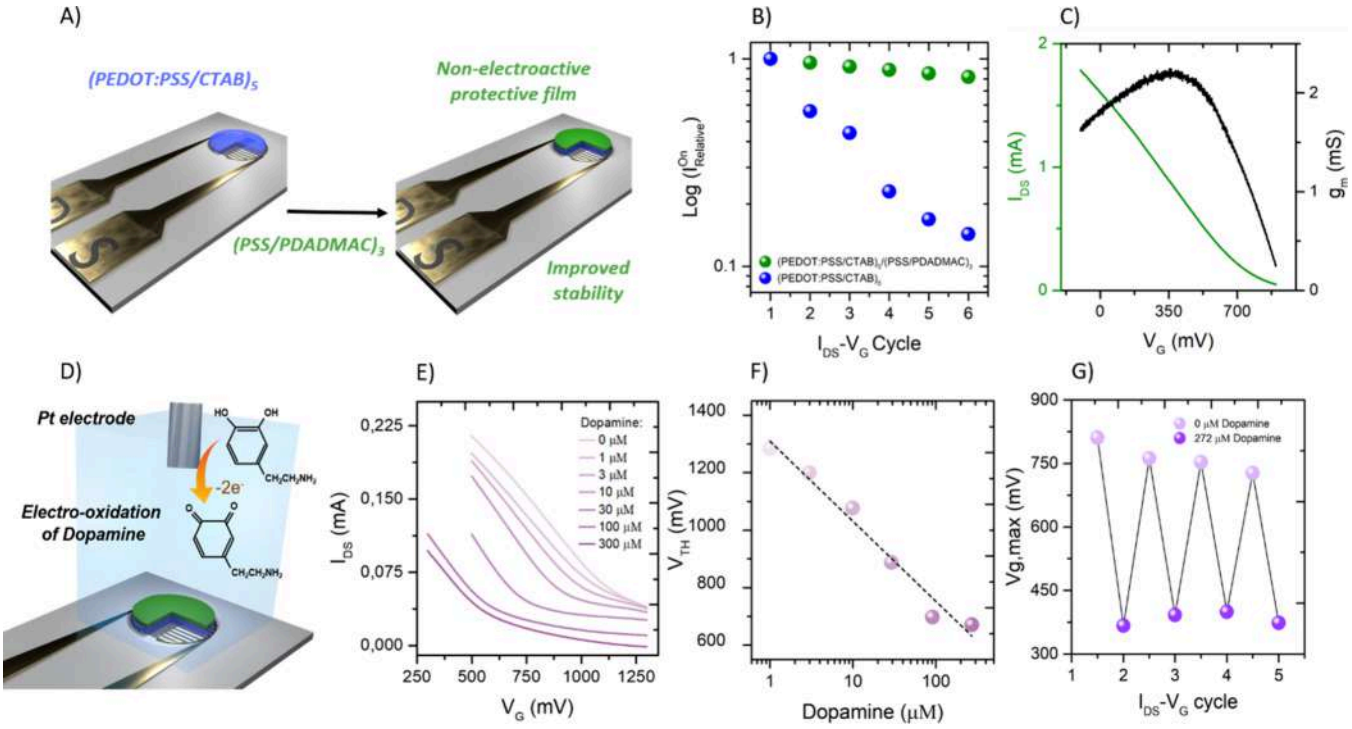

Figure 5. (A) Schematic representation of $(PEDOT:PSS/CTAB)_7$ (left) and $(PEDOT:PSS/CTAB)_5/(PSS/PDADMAC)_3$ (right) OECTs. (B) Relative maximum current ($I_{Rel,on}$) as a function of the number of transfer curves carried for the $(PEDOT:PSS/CTAB)_5$ (blue) and $(PEDOT:PSS/CTAB)_5/(PSS/PDADMAC)_3$ (green) OECTs. (C) I_{DS} (green) and transconductance (black) as a function of V_G for a $(PEDOT:PSS/CTAB)_5/(PSS/PDADMAC)_3$ film. Measured with a V_{DS} of 700 mV and at a sweep speed of 10 mV/s. (D) Dopamine detection representation scheme. (E) Transfer curves for different concentrations of dopamine, from 0 to 300 μM. The curves were measured applying a scan rate of 50 mV/s and a V_{DS} of 100 mV. (F) Threshold potential (V_{TH}) as a function of dopamine concentration obtained from their respective transfer curves. The dashed line is the linear fit. (G) Reversibility of the dopamine detection system. $V_{g,max}$ as a function of the number of cycles of transfer curves going from a solution in the absence of dopamine to a 272 μM dopamine solution. All of the OECT experiments were done in the presence of 0.1 M KCl.

number of assembled bilayers (Figure 4B). It should be noted that for these systems the gate−source current (I_{GS}) measured during the transfer characteristic curves had negligible values compared to I_{DS} (see Figure S7), which evidence a very low leakage current rate. On the other hand, the $(PEDOT:PSS/PDADMAC)_n$ films show very low I_{DS} and practically the same as I_{GS} (see Figure S9), evidencing that for these systems (n = 3, 5, and 7) the leakage current governs the current measured in the OECT.

In terms of transistor channel design and fabrication, the LbL nanoconstruction technique is very attractive because it offers a simple strategy to control the film thickness with nanometer precision without the requirement of complex equipment. Figure 4B also shows the transconductance as a function of the gate potential of the assemblies $(PEDOT:PSS/CTAB)_n$ for n = 3, 5, and 7. The transconductance g_m increases with the number of bilayers. By comparison of g_m with the ellipsometric film thicknesses (Figure 4C), g_m follows an

https://doi.org/10.1021/acsaelm.3c01592
ACS Appl. Electron. Mater. 2024, 6, 1211−1222

exponential increase in good concordance with the electrical conductance results.

One of the main drawbacks of some PEDOT-based OECTs is that they could demand the use of high gate voltages (≈0.8 V vs Ag/AgCl) to maintain the channel in the OFF condition (i.e., OECTs with high V_{TH}). This relatively high V_G can trigger parasitic reactions with water and oxygen, prompting device deterioration.[35,54] For $(PEDOT:PSS/CTAB)_n$, V_{TH} ranges from 0.369 V (n = 3) to 0.426 V (n = 7) (Table S1). Thus, our construction approach allows tuning not only the g_m but also the V_{TH} (and the potential of maximum transconductance, $V_{g,max}$) by the number of bilayers. For some electrolyte compositions, OECTs with low V_{TH} values are required to avoid the oxygen reduction reaction. In this case, the OECTs $n \leq 3$ should be used. On the other hand, for (bio)sensing applications OECTs with high transconductance are preferred to develop sensors with greater sensitivity.[55] Here, transistors with $n \geq 5$ should be used.

In order to evaluate the cycling stability of OECTs prepared with PEDOT:PSS/CTAB films, six successive measurements of characteristic transfer curves were performed (Figure S10). A decrease in current is observed with each new measurement cycle due to a loss of electroactivity of the film. After six $I_{DS}-V_G$ curves, approximately 90% of the transistor current was lost. Although not desired, the loss of activity in OECTs during cycling is a fairly common phenomenon and was explained by the alteration of the nano/micro structure or material loss of the conducting film due to ionic charge transport and/or electrochemical side reactions.[56,57] For example, the PIBET-BO OECTs showed an irreversible loss of approximately 50% of the current after five ON−OFF cycles. On the other hand, OECTs made of the PIBT-BO conductive film showed a loss of 50% of the current in 11 ON−OFF cycles.[58] Giovannitti et al. reported that cycling stability is reduced considerably if the OECT is measured applying large gate potentials such as during our $I_{DS}-V_G$ curves.[57] In OECTs devices, current modulation occurs simultaneously with ions penetrating the bulk of the channel material. As described by Xie et al.,[52] the entry/egress of (hydrated) ions in the bulk of conducting film would cause obvious changes on the micro/nano structure. Consequently, during repeated doping/dedoping processes through V_G modulation, the dynamic swelling/deswelling of the polymer film would continuously deteriorate its micro/nano structure. In addition, the swelling of an electroactive polymer film could lead to some loss of the components. Both events can be considerably reduced by nanoarchitectonic engineering. This behavior can be a limiting factor in the use of these devices for various applications because a transistor with good functional stability is desired. As reported by other authors, the stability of LbL assemblies can be enhanced by the deposition of an outer layer that acts as a "protection" of the underling components.[59,60] For example, an assembly of nonelectroactive polyelectrolyte outer film was employed to increase the stability of a redox polymer multilayer film.[58]

Therefore, we prepared an outer nonconducting coating by LbL assembly of the polycation PDADMAC and the polyanion PSS on top of the conducting channel to improve the mechanical stability of the PEDOT-based assembly. This outer film was prepared by assembling 3 bilayers of PSS/PDADMAC (Figure 5A), which resulted in an extra thickness of 11 nm (see the Supporting Information and Figure S11 for more details). If no protective layer is used, the thickness of the $(PEDOT:PSS/CTAB)_5$ film decreases by 20% after six electrochemical measurements. However, it was found that the use of the outer layer prevented the thickness decrease, retaining 95% of the original thickness of the $(PEDOT:PSS/CTAB)_5(PSS/PDADMAC)_3$ assembly after the same number of cycles. These results would indicate that the protective layer reduces the alteration of the micro/nano structure of the PEDOT:PSS/CTAB film during doping/dedoping processes. A decrease of both the swelling and the loss of film components may explain the enhancement of the electroactive stability. In order to evaluate the implication of the outer film on the field effect properties of a $(PEDOT:PSS/CTAB)_5$ OECT, transfer characteristic curves were performed before and after functionalization (Figure S12). After the outer layer was prepared, $V_{g,max}$ changes from 95 to 155 mV. To evaluate the electrochemical stability properties of the outer film, an OECT of $(PEDOT:PSS/CTAB)_5$ modified with $(PSS/PDADMAC)_3$ was prepared, and $I_{DS}-V_G$ cycles were performed (Figure S13). For a direct comparison against the system without the protection film, the relative current ($I_{rel} = I_{on(x)}/I_{on(1)}$) is plotted against the number of cycles for both systems in Figure 5B. In the case of the film $(PEDOT:PSS/CTAB)_5/(PSS/PDADMAC)_3$, the I_{max} decreased by 3% per cycle, whereas in the system $(PEDOT:PSS/CTAB)_5$ decreased 15% per cycle. These results show that the protective film significantly improves the cycling stability of the OECT.

The transfer characteristics of the $(PEDOT:PSS/CTAB)_5$-$(PSS/PDADMAC)_3$ OECT were also studied (Figure 5C). A $g_{m,max}$ value of 2.21 mS was obtained at a V_G = 350 mV. As was described by Rivnay and co-workers,[55] the OECTs transconductance for organic film thickness up to 1 μm is given by

$$g_m = \left(\frac{Wd}{L}\right)\mu C^*(V_{TH} - V_G) \quad (1)$$

where W is the width, L is the length, and d is the thickness of the transistor channel. Furthermore, μ is the hole mobility of the film, C^* is the capacitance per unit of volume, and V_{TH} is a geometry-independent threshold voltage. By introducing the $g_{m,max}$ and the ellipsometric film thickness in eq 1, the μC^* constant was estimated with a value of 0.23 F cm^{-1} V^{-1} s^{-1}. This value is comparable to those obtained for electrolyte gated OECTs of PEDOT doped with anionic polyelectrolyte dopants with methacrylic backbone.[14,61] Furthermore, the output characteristics of the $(PEDOT:PSS/CTAB)_5(PSS/PDADMAC)_3$ OECT showed a typical depletion-mode behavior for $V_{DS} > 0$ (Figure S14).[62,63]

Finally, the kinetics involved in the on−off process of the OECTs was also studied. The transient performance is a crucial characteristic of these devices in applications such as (bio)sensing, and it was studied using a potential pulse leading the system from the on-state (I_{on}) to the off-state (I_{off}). A square pulse potential of 3 s was applied from 700 mV (off-state) to −350 mV (on-state) versus a Ag/AgCl gate. The turn-on (τ_{on}) and turn-off (τ_{off}) characteristic times were obtained from exponential fits. The transient response of assembled $(PEDOT:PSS/CTAB)_5/(PSS/PDADMAC)_3$ is shown in Figure S15. The τ_{on} and τ_{off} calculated values are 24.2 ± 0.4 and 12.3 ± 6.4 ms, respectively (Table 2). It should be noted that these values are lower than those reported for OECTs prepared by other PEDOT-based films[35,64] and similar to fast-response OECTs.[65]

Biosensing of Dopamine with PEDOT:PSS/CTAB OECTs. To prove the viability of the LbL-prepared OECTs for developing functional biosensors, we evaluated the

https://doi.org/10.1021/acsaelm.3c01592
ACS Appl. Electron. Mater. 2024, 6, 1211−1222

Table 2. Kinetic Parameters Obtained from the Transient Response of the OECTs Prepared in This Work and Their Comparison with PEDOT-Based Transistors Previously Reported

OECT film	τ_{on} (ms)	τ_{off} (ms)	ref
$(PEDOT:PSS/CTAB)_5$	33.3 ± 5.5	19.2 ± 1.3	this work
$(PEDOT:PSS/CTAB)_5/(PSS/PDADMAC)_3$	24.2 ± 0.4	12.3 ± 6.4	this work
PEDOT/PAH	115	125	35
PEDOT-S:$(Oct)_2NH_2$	87 ± 59	23 ± 12	64
PEDOT-S:$(Nonyl)NH_3$	146 ± 46	24 ± 14	64
PEDOT:PSS/TX	6.8	11	65

bioelectronic detection of dopamine (Figure 5D), a vital neurotransmitter with crucial roles in the central nervous system and hormonal regulation,[66] using the $(PEDOT:PSS/CTAB)_5/(PSS/PDADMAC)_3$ as conducting channel. Imbalances or malfunctions in dopaminergic neuronal processing can contribute to various neurological conditions, including sleeping and eating disorders, Parkinson's disease, and addictive behaviors linked to drug abuse. However, detecting dopamine in biological systems remains a challenge due to its low clinical concentrations, such as nanomolar in plasma and micromolar in urine.[67] Consequently, rapid and accurate dopamine detection holds immense importance for routine analysis and neurological disorder diagnosis.[68]

Transfer characteristics curves were measured for incremental concentrations of dopamine (Figure 5E) by using a $(PEDOT:PSS/CTAB)_5/(PSS/PDADMAC)_3$ OECT with a Pt gate electrode. Curves show a shift of V_{TH} toward more negative V_G potentials as the dopamine concentration increases. The response of the transistor is due to the electrochemical reaction of dopamine at the gate, that is, the electro-oxidation to *o*-dopaminequinone, yielding large variations of the effective gate voltage (V_G^{eff}).[67,69] As previously reported, V_G^{eff} can be described as follows:

$$V_G^{eff} = V_G + 2.3(1+\gamma)\frac{kT}{ne}\log(C_{dopamine}) + A \quad (2)$$

where V_G is the gate voltage without dopamine, γ the capacitance ratio (defined as C_C/C_G, which are the channel and gate capacitance, respectively), k the Boltzmann constant, T the temperature, e the elementary charge, n the number of electrons transferred during the electro-oxidation of dopamine ($n = 2$), and A a constant related to other factors. From this equation, the V_{TH} shift (ΔV_{TH}) can be expressed as

$$\Delta V_{TH} = 2.3(1+\gamma)\frac{kT}{ne}\log(C_{dopamine}) \quad (3)$$

Figure 5F shows ΔV_{TH} as a function of $\log(C_{dopamine})$, and a linear dependence is observed for a range of 1−300 μM. The slope of the fitting curve is 279 mV/decade, and by using eq 3, γ was calculated and a value of 8.44 was obtained. Our value is higher than those reported by Tang et al.[67] and similar to those reported by Liao et al.[70] In addition, the sensitivity obtained in this work (279 mV/decade) is many times higher than those reported for the detection of sialic acid (57.5 mV/decade) using another LbL OECT system.[27] The reversibility of the LbL-based OECT biosensor was studied by measuring several times the $I_{DS}-V_G$ curves in the absence and presence of 300 μM dopamine. V_{TH} values are shown in Figure 5G and evidence very good reversibility of the sensing device.

CONCLUSIONS

We have introduced a supramolecular fabrication approach with simple equipment for the preparation of conducting polymer films based on poly(3,4-ethylenedioxythiophene):poly(styrenesulfonate) (PEDOT:PSS) integrated with cationic molecular building blocks through layer-by-layer (LbL) self-assembly for being applied in OECT devices. The incorporation of cetyltrimethylammonium bromide (CTAB) into PEDOT:PSS resulted in a four-order-of-magnitude increase in conductance compared to the integration with poly(diallyldimethylammonium chloride) (PDADMAC). This enhancement can be attributed to the positive effect of CTAB on charge transport within the PEDOT:PSS matrix. These results are very important as the use of CTAB may improve the performance of the systems and applications in which LbL made of PEDOT:PSS/polycations were used.[27,71,72] We have also demonstrated that the LbL assembly of PEDOT:PSS and CTAB allows the tunability of key electronic performance indicators of the OECTs, such as current at the on-state (I_{max}), threshold potential (V_{TH}), and transconductance (g_m), by adjusting the thickness of the transistor channel film. This tunability provides flexibility for tailoring OECTs to specific applications. On the other hand, the incorporation of a protective capping through further LbL assembly of nonelectroactive polymers has significantly improved the cycling stability of the OECT transistor channel without affecting the charge transport processes of the underlying conducting channel, which becomes crucial for long-term device functionality. Furthermore, we have illustrated the practical utility of these prepared OECTs in biosensing applications, specifically for detecting the neurotransmitter dopamine. These OECTs exhibit exceptional sensitivity, a wide operational range, and reversibility in biosensing, highlighting their potential for biomedical and healthcare applications. Finally, we hope the present results will pave the way to further studies in which the advantages of the LbL assembly, such as the precise control of film thickness and composition, can be exploited to the next level for producing active channels for field effect devices.

ASSOCIATED CONTENT

Supporting Information

The Supporting Information is available free of charge at https://pubs.acs.org/doi/10.1021/acsaelm.3c01592.

Materials and method information, UV−vis spectroscopic results, ellipsometric results and analysis, additional electrochemical characterization, and transient response of OECTs (PDF)

AUTHOR INFORMATION

Corresponding Authors

Esteban Piccinini − *Instituto de Investigaciones Fisicoquímicas Teóricas y Aplicadas (INIFTA), Departamento de Química, Facultad de Ciencias Exactas, Universidad Nacional de La Plata, La Plata B1904DPI, Argentina;* orcid.org/0000-0003-3270-7150; Email: estebanpiccinini@inifta.unlp.edu.ar

Waldemar A. Marmisollé − *Instituto de Investigaciones Fisicoquímicas Teóricas y Aplicadas (INIFTA),*

https://doi.org/10.1021/acsaelm.3c01592
ACS Appl. Electron. Mater. 2024, 6, 1211−1222

Departamento de Química, Facultad de Ciencias Exactas, Universidad Nacional de La Plata, La Plata B1904DPI, Argentina; orcid.org/0000-0003-0031-5371; Email: wmarmi@inifta.unlp.edu.ar

Authors

Joaquin F. Diforti − *Instituto de Investigaciones Fisicoquímicas Teóricas y Aplicadas (INIFTA), Departamento de Química, Facultad de Ciencias Exactas, Universidad Nacional de La Plata, La Plata B1904DPI, Argentina*

Juan A. Allegretto − *Instituto de Investigaciones Fisicoquímicas Teóricas y Aplicadas (INIFTA), Departamento de Química, Facultad de Ciencias Exactas, Universidad Nacional de La Plata, La Plata B1904DPI, Argentina; Laboratory for Life Sciences and Technology (LiST), Faculty of Medicine and Dentistry, Danube Private University, 3500 Krems, Austria;* orcid.org/0000-0002-7371-2610

Catalina von Bilderling − *Instituto de Investigaciones Fisicoquímicas Teóricas y Aplicadas (INIFTA), Departamento de Química, Facultad de Ciencias Exactas, Universidad Nacional de La Plata, La Plata B1904DPI, Argentina;* orcid.org/0000-0002-4913-5307

Omar Azzaroni − *Instituto de Investigaciones Fisicoquímicas Teóricas y Aplicadas (INIFTA), Departamento de Química, Facultad de Ciencias Exactas, Universidad Nacional de La Plata, La Plata B1904DPI, Argentina;* orcid.org/0000-0002-5098-0612

Complete contact information is available at: https://pubs.acs.org/10.1021/acsaelm.3c01592

Notes

The authors declare no competing financial interest.

■ ACKNOWLEDGMENTS

This work was supported by the following institutions: Universidad Nacional de La Plata (UNLP, PID-X867), ANPCYT (PICT 2018-04684, PICT-2021-GRF-TI-00042). E.P., W.A.M., C.V.B., and O.A. are staff members of CONICET. J.A.A. and J.F.D. acknowledge their fellowships from CONICET.

■ REFERENCES

(1) Han, M.; Chen, L.; Aras, K.; Liang, C.; Chen, X.; Zhao, H.; Li, K.; Faye, N. R.; Sun, B.; Kim, J. H.; Bai, W.; Yang, Q.; Ma, Y.; Lu, W.; Song, E.; Baek, J. M.; Lee, Y.; Liu, C.; Model, J. B.; Rogers, J. A.; et al. Catheter-Integrated Soft Multilayer Electronic Arrays for Multiplexed Sensing and Actuation during Cardiac Surgery. *Nat. Biomed. Eng.* **2020**, *4* (10), 997−1009.

(2) Patch, K. Neural Dust Swept up in Latest Leap for Bioelectronic Medicine. *Nat. Biotechnol.* **2021**, *39* (3), 255−256.

(3) Jin, F.; Li, T.; Wei, Z.; Xiong, R.; Qian, L.; Ma, J.; Yuan, T.; Wu, Q.; Lai, C.; Ma, X.; Wang, F.; Zhao, Y.; Sun, F.; Wang, T.; Feng, Z. Biofeedback Electrostimulation for Bionic and Long-Lasting Neural Modulation. *Nat. Commun.* **2022**, *13* (1), 5302.

(4) Simon, D. T.; Gabrielsson, E. O.; Tybrandt, K.; Berggren, M. Organic Bioelectronics: Bridging the Signaling Gap between Biology and Technology. *Chem. Rev.* **2016**, *116* (21), 13009−13041.

(5) Van De Burgt, Y.; Melianas, A.; Keene, S. T.; Malliaras, G.; Salleo, A. Organic Electronics for Neuromorphic Computing. *Nat. Electron.* **2018**, *1* (7), 386−397.

(6) Keene, S. T.; Fogarty, D.; Cooke, R.; Casadevall, C. D.; Salleo, A.; Parlak, O. Wearable Organic Electrochemical Transistor Patch for Multiplexed Sensing of Calcium and Ammonium Ions from Human Perspiration. *Adv. Healthc. Mater.* **2019**, *8* (24), 1−8.

(7) Fenoy, G. E.; Hasler, R.; Quartinello, F.; Marmisollé, W. A.; Lorenz, C.; Azzaroni, O.; Bäuerle, P.; Knoll, W. Clickable" Organic Electrochemical Transistors. *JACS Au* **2022**, *2* (12), 2778−2790.

(8) Huang, W.; Chen, J.; Yao, Y.; Zheng, D.; Ji, X.; Feng, L.-W.; Moore, D.; Glavin, N. R.; Xie, M.; Chen, Y.; Pankow, R. M.; Surendran, A.; Wang, Z.; Xia, Y.; Bai, L.; Rivnay, J.; Ping, J.; Guo, X.; Cheng, Y.; Marks, T. J.; Facchetti, A. Vertical Organic Electrochemical Transistors for Complementary Circuits. *Nature* **2023**, *613* (7944), 496−502.

(9) Fenoy, G. E.; Hasler, R.; Lorenz, C.; Movilli, J.; Marmisollé, W. A.; Azzaroni, O.; Huskens, J.; Bäuerle, P.; Knoll, W. Interface Engineering of "Clickable" Organic Electrochemical Transistors toward Biosensing Devices. *ACS Appl. Mater. Interfaces* **2023**, *15* (8), 10885−10896.

(10) Zeglio, E.; Inganäs, O. Active Materials for Organic Electrochemical Transistors. *Adv. Mater.* **2018**, *30* (44), 1−18.

(11) Gueye, M. N.; Carella, A.; Faure-Vincent, J.; Demadrille, R.; Simonato, J. P. Progress in Understanding Structure and Transport Properties of PEDOT-Based Materials: A Critical Review. *Prog. Mater. Sci.* **2020**, *108*, 100616.

(12) Donahue, M. J.; Sanchez-Sanchez, A.; Inal, S.; Qu, J.; Owens, R. M.; Mecerreyes, D.; Malliaras, G. G.; Martin, D. C. Tailoring PEDOT Properties for Applications in Bioelectronics. *Materials Science and Engineering R: Reports.* **2020**, *140*, 100546.

(13) Sappia, L. D.; Piccinini, E.; von Binderling, C.; Knoll, W.; Marmisollé, W.; Azzaroni, O. PEDOT-Polyamine Composite Films for Bioelectrochemical Platforms - Flexible and Easy to Derivatize. *Mater. Sci. Eng., C* **2020**, *109*, 110575.

(14) Inal, S.; Malliaras, G. G.; Rivnay, J. Benchmarking Organic Mixed Conductors for Transistors. *Nat. Commun.* **2017**, *8* (1), 1−6.

(15) Cicoira, F.; Sessolo, M.; Yaghmazadeh, O.; Defranco, J. A.; Yang, S. Y.; Malliaras, G. C. Influence of Device Geometry on Sensor Characteristics of Planar Organic Electrochemical Transistors. *Adv. Mater.* **2010**, *22* (9), 1012−1016.

(16) Hui, Y.; Bian, C.; Xia, S.; Tong, J.; Wang, J. Synthesis and Electrochemical Sensing Application of Poly(3,4-Ethylenedioxythiophene)-Based Materials: A Review. *Anal. Chim. Acta* **2018**, *1022*, 1−19.

(17) Kim, C.; Azimi, M.; Fan, J.; Nagarajan, H.; Wang, M.; Cicoira, F. All-Printed and Stretchable Organic Electrochemical Transistors Using a Hydrogel Electrolyte. *Nanoscale* **2023**, *15*, 3263−3272.

(18) Azzaroni, O.; Ariga, K. *Materials Nanoarchitectonics: From Integrated Molecular Systems to Advanced Devices*; Azzaroni, O., Ariga, K., Eds.; Elsevier: 2024.

(19) Azzaroni, O.; Ariga, K. *Concepts and Design of Materials Nanoarchitectonics*, 1st ed.; Azzaroni, O., Ariga, K., Eds.; Royal Society of Chemistry: 2022.

(20) Decher, G.; Schlenoff, J. B. *Multilayer Thin Films: Sequential Assembly of Nanocomposite Materials*, 2nd ed.; Decher, G., Schlenoff, J. B., Eds.; WILEY-VCH Verlag GmbH & Co: 2012.

(21) Zhao, S.; Caruso, F.; Dahne, L.; Decher, G.; De Geest, B. G.; Fan, J.; Feliu, N.; Gogotsi, Y.; Hammond, P. T.; Hersam, M. C.; Khademhosseini, A.; Kotov, N.; Leporatti, S.; Li, Y.; Lisdat, F.; Liz-Marzan, L. M.; Moya, S.; Mulvaney, P.; Rogach, A. L.; Parak, W. J.; et al. The Future of Layer-by-Layer Assembly: A Tribute to ACS Nano Associate Editor Helmuth Mohwald. *ACS Nano* **2019**, *13* (6), 6151−6169.

(22) Dubas, S. T.; Schlenoff, J. B. Factors Controlling the Growth of Polyelectrolyte Multilayers. *Macromolecules* **1999**, *32* (24), 8153−8160.

(23) Azzaroni, O.; Piccinini, E.; Fenoy, G. E.; Marmisollé, W. A.; Ariga, K. Field-Effect Transistors Engineered via Solution-Based Layer-by-Layer Nanoarchitectonics. *Nanotechnology* **2023**, *34*, 472001.

(24) David, M.; Barsan, M. M.; Brett, C. M. A.; Florescu, M. Improved Glucose Label-Free Biosensor with Layer-by-Layer

Architecture and Conducting Polymer Poly(3,4-Ethylenedioxythiophene). *Sensors Actuators, B Chem.* **2018**, *255*, 3227−3234.
(25) Pappa, A. M.; Inal, S.; Roy, K.; Zhang, Y.; Pitsalidis, C.; Hama, A.; Pas, J.; Malliaras, G. G.; Owens, R. M. Polyelectrolyte Layer-by-Layer Assembly on Organic Electrochemical Transistors. *ACS Appl. Mater. Interfaces* **2017**, *9* (12), 10427−10434.
(26) Fenoy, G. E.; Scotto, J.; Allegretto, J. A.; Piccinini, E.; Cantillo, A. L.; Knoll, W.; Azzaroni, O.; Marmisollé, W. A. Layer-by-Layer Assembly Monitored by PEDOT-Polyamine-Based Organic Electrochemical Transistors. *ACS Appl. Electron. Mater.* **2022**, *4* (12), 5953−5962.
(27) Zhu, R.; Wang, Y.; Tao, Y.; Wang, Y.; Chen, Y.; Li, M.; Liu, Q.; Yang, L.; Wang, D. Layer-by-Layer Assembly of Composite Conductive Fiber-Based Organic Electrochemical Transistor for Highly Sensitive Detection of Sialic Acid. *Electrochim. Acta* **2022**, *425*, 140716.
(28) Groenendaal, B. L.; Jonas, F.; Freitag, D.; Pielartzik, H.; Reynolds, J. R. Poly(3,4-Ethylenedioxythiophene) and Its Derivatives: Past, Present, and Future. *Adv. Mater.* **2000**, *12*, 481−494.
(29) Piccinini, E.; Ceolín, M.; Battaglini, F.; Azzaroni, O. Mesostructured Electroactive Thin Films Through Layer-by-Layer Assembly of Redox Surfactants and Polyelectrolytes. *ChemPlusChem.* **2020**, *85* (8), 1616−1622.
(30) Piccinini, E.; González, G. A.; Azzaroni, O.; Battaglini, F. Mass and Charge Transport in Highly Mesostructured Polyelectrolyte/Electroactive-Surfactant Multilayer Films. *J. Colloid Interface Sci.* **2021**, *581*, 595−607.
(31) Arys, X.; Fischer, P.; Jonas, A. M.; Koetse, M. M.; Laschewsky, A.; Legras, R.; Wischerhoff, E. Ordered Polyelectrolyte Multilayers. Rules Governing Layering in Organic Binary Multilayers. *J. Am. Chem. Soc.* **2003**, *125* (7), 1859−1865.
(32) Cortez, M. L.; De Matteis, N.; Ceolín, M.; Knoll, W.; Battaglini, F.; Azzaroni, O. Hydrophobic Interactions Leading to a Complex Interplay between Bioelectrocatalytic Properties and Multilayer Meso-Organization in Layer-by-Layer Assemblies. *Phys. Chem. Chem. Phys.* **2014**, *16*, 20844−20855.
(33) Cortez, M. L.; Ceolín, M.; Camacho, L. C.; Donath, E.; Moya, S. E.; Battaglini, F.; Azzaroni, O. Solvent Effects on the Structure-Property Relationship of Redox-Active Self-Assembled Nanoparticle-Polyelectrolyte-Surfactant Composite Thin Films: Implications for the Generation of Bioelectrocatalytic Signals in Enzyme-Containing Assemblies. *ACS Appl. Mater. Interfaces* **2017**, *9* (1), 1119−1128.
(34) Yeon, C.; Kim, G.; Lim, J. W.; Yun, S. J. Highly conductive PEDOT:PSS treated by sodium dodecyl sulfate for stretchable fabric heaters. *RSC Adv.* **2017**, *7* (10), 5888−5897.
(35) Fenoy, G. E.; von Bilderling, C.; Knoll, W.; Azzaroni, O.; Marmisolle, W. A. PEDOT:Tosylate-Polyamine-Based Organic Electrochemical Transistors for High-Performance Bioelectronics. *Adv. Electron. Mater.* **2021**, *7*, 2100059.
(36) Jurin, F. E.; Buron, C. C.; Martin, N.; Filiâtre, C. Preparation of Conductive PDDA/(PEDOT: PSS) Multilayer Thin Film: Influence of Polyelectrolyte Solution Composition. *J. Colloid Interface Sci.* **2014**, *431*, 64−70.
(37) Montero-Jimenez, M.; Amante, F. L.; Fenoy, G. E.; Scotto, J.; Azzaroni, O.; Marmisolle, W. A. PEDOT-Polyamine-Based Organic Electrochemical Transistors for Monitoring Protein Binding. *Biosensors* **2023**, *13* (2), 288.
(38) Jurin, F. E.; Buron, C. C.; Martin, N.; Monney, S.; Filiâtre, C. Electrical Conductivity Enhancement and Wettability Modification of (PDDA/PEDOT:PSS)n Multilayer Film. *Thin Solid Films* **2018**, *664*, 33−40.
(39) Sappia, L. D.; Piccinini, E.; Marmisollé, W.; Santilli, N.; Maza, E.; Moya, S.; Battaglini, F.; Madrid, R. E.; Azzaroni, O. Integration of Biorecognition Elements on PEDOT Platforms through Supramolecular Interactions. *Adv. Mater. Interfaces* **2017**, *4* (17), 1700502.
(40) Piccinini, E.; Tuninetti, J. S.; Irigoyen Otamendi, J.; Moya, S. E.; Ceolín, M.; Battaglini, F.; Azzaroni, O. Surfactants as Mesogenic Agents in Layer-by-Layer Assembled Polyelectrolyte/Surfactant Multilayers: Nanoarchitectured "Soft" Thin Films Displaying a Tailored Mesostructure. *Phys. Chem. Chem. Phys.* **2018**, *20* (14), 9298−9308.
(41) Guzman, E.; Ritacco, H.; Ortega, F.; Svitova, T.; Radke, C. J.; Rubio, R. G. Adsorption Kinetics and Mechanical Properties of Ultrathin Polyelectrolyte Multilayers: Liquid-Supported versus Solid-Supported Films. *J. Phys. Chem. B* **2009**, *113*, 7128−7137.
(42) Okutan, M.; Deligöz, H. Effect of External Salt Addition on the Structural, Morphological and Electrochemical Properties of Flexible PEDOT: PSS Based LbL Multilayered Films. *Colloids Surfaces A* **2019**, *580*, 123695.
(43) Tang, Z.; Donohoe, S. T.; Robinson, J. M.; Chiarelli, P. A.; Wang, H. Film Formation, Surface Character, and Relative Density for Electrochromic PEI /(PSS: PEDOT) Multilayered Thin Films. *Polymer* **2005**, *46*, 9043−9052.
(44) Scotto, J.; Cantillo, A. L.; Piccinini, E.; Fenoy, G. E.; Allegretto, J. A.; Piccinini, J. M.; Marmisollé, W. A.; Azzaroni, O. Using Graphene Field-Effect Transistors for Real-Time Monitoring of Dynamic Processes at Sensing Interfaces. Benchmarking Performance against Surface Plasmon Resonance. *ACS Appl. Electron. Mater.* **2022**, *4* (8), 3988−3996.
(45) Garreau, S.; Louarn, G.; Buisson, J. P.; Froyer, G.; Lefrant, S. In Situ Spectroelectrochemical Raman Studies of Poly(3,4-Ethylenedioxythiophene) (PEDT). *Macromolecules* **1999**, *32* (20), 6807−6812.
(46) Schaarschmidt, A.; Farah, A. A.; Aby, A.; Helmy, A. S. Influence of Nonadiabatic Annealing on the Morphology and Molecular Structure of PEDOT−PSS Films. *J. Phys. Chem. B* **2009**, *113* (28), 9352−9355.
(47) Yu, C.; Varghese, L.; Irudayaraj, J. Surface Modification of Cetyltrimethylammonium Bromide-Capped Gold Nanorods to Make Molecular Probes. *Langmuir* **2007**, *23* (17), 9114−9119.
(48) Lorenzo, A.; Marmisollé, W. A.; Maza, E. M.; Ceolín, M.; Azzaroni, O. Electrochemical Nanoarchitectonics through Polyaminobenzylamine-Dodecyl Phosphate Complexes: Redox Activity and Mesoscopic Organization in Self-Assembled Nanofilms. *Phys. Chem. Chem. Phys.* **2018**, *20* (11), 7570−7578.
(49) Dane, T. G.; Cresswell, P. T.; Pilkington, G. A.; Lilliu, S.; Macdonald, J. E.; Prescott, S. W.; Bikondoa, O.; Faul, D. C. F. J.; Briscoe, W. H. Oligo(Aniline) Nanofilms: From Molecular Architecture to Microstructure. *Soft Matter* **2013**, *9*, 10501−10511.
(50) Olinga, T. E.; Fraysse, J.; Travers, J. P.; Dufresne, A.; Pron, A. Highly Conducting and Solution-Processable Polyaniline Obtained via Protonation with a New Sulfonic Acid Containing Plasticizing Functional Groups. *Macromolecules* **2000**, *33*, 2107−2113.
(51) Jurin, F. E.; Buron, C. C.; Clément, S.; Mehdi, A.; Viau, L.; Lakard, B.; Martin, N.; Filiâtre, C. Flexible and Conductive Multilayer Films Based on the Assembly of PEDOT:PSS and Water Soluble Polythiophenes. *Org. Electron.* **2017**, *46*, 263−269.
(52) Cutler, C. A.; Bouguettaya, M.; Reynolds, J. R. PEDOT Polyelectrolyte Based Electrochromic Films via Electrostatic Adsorption. *Adv. Mater.* **2002**, *14* (9), 684−688.
(53) Paulsen, B. D.; Tybrandt, K.; Stavrinidou, E.; Rivnay, J. Organic Mixed Ionic−Electronic Conductors. *Nat. Mater.* **2020**, *19* (1), 13−26.
(54) Keene, S. T.; van der Pol, T. P. A.; Zakhidov, D.; Weijtens, C. H. L.; Janssen, R. A. J.; Salleo, A.; van de Burgt, Y. Enhancement-Mode PEDOT:PSS Organic Electrochemical Transistors Using Molecular De-Doping. *Adv. Mater.* **2020**, *32* (19), 2000270.
(55) Rivnay, J.; Leleux, P.; Ferro, M.; Sessolo, M.; Williamson, A.; Koutsouras, D. A.; Khodagholy, D.; Ramuz, M.; Strakosas, X.; Owens, R. M.; Benar, C.; Badier, J. M.; Bernard, C.; Malliaras, G. G. High-Performance Transistors for Bioelectronics through Tuning of Channel Thickness. *Sci. Adv.* **2015**, *1* (4), 1−6.
(56) Xie, M.; Liu, H.; Wu, M.; Chen, C.; Wen, J.; Bai, L.; Yu, J.; Huang, W. Cycling Stability of Organic Electrochemical Transistors. *Org. Electron.* **2023**, *117*, 106777.
(57) Giovannitti, A.; Rashid, R. B.; Thiburce, Q.; Paulsen, B. D.; Cendra, C.; Thorley, K.; Moia, D.; Mefford, J. T.; Hanifi, D.; Weiyuan, D.; Moser, M.; Salleo, A.; Nelson, J.; Mcculloch, I.; Rivnay,

https://doi.org/10.1021/acsaelm.3c01592
ACS Appl. Electron. Mater. 2024, 6, 1211−1222

J. Energetic Control of Redox-Active Polymers toward Safe Organic Bioelectronic Materials. *Advanced Materials* **2020**, *32*, 1−9.
(58) Wang, Y.; Zeglio, E.; Liao, H.; Jinqiu, Xu; Liu, F.; Li, Z.; et al. Iuliana Petruta Maria, Damia Mawad, Anna Herland, Iain McCulloch, and Wan Yue, Hybrid Alkyl−Ethylene Glycol Side Chains Enhance SubstrateAdhesion and Operational Stability in Accumulation Mode OrganicElectrochemical Transistors. *Chem. Mater.* **2019**, *31* (23), 9797−9806.
(59) Song, J.; Jańczewski, D.; Ma, Y.; Hempenius, M.; Xu, J.; Vancso, G. J. Disassembly of Redox Responsive Poly-(Ferrocenylsilane) Multilayers: The Effect of Blocking Layers, Supporting Electrolyte and Polyion Molar Mass. *J. Colloid Interface Sci.* **2013**, *405*, 256−261.
(60) Michel, M.; Izquierdo, A.; Decher, G.; Voegel, J. C.; Schaaf, P.; Ball, V. Layer by Layer Self-Assembled Polyelectrolyte Multilayers with Embedded Phospholipid Vesicles Obtained by Spraying: Integrity of the Vesicles. *Langmuir* **2005**, *21* (17), 7854−7859.
(61) Inal, S.; Rivnay, J.; Hofmann, A. I.; Uguz, I.; Mumtaz, M.; Katsigiannopoulos, D.; Brochon, C.; Cloutet, E.; Hadziioannou, G.; Malliaras, G. G. Organic Electrochemical Transistors Based on PEDOT with Different Anionic Polyelectrolyte Dopants. *J. Polym. Sci., Part B: Polym. Phys.* **2016**, *54* (2), 147−151.
(62) Tarabella, G.; D'Angelo, P.; Cifarelli, A.; Dimonte, A.; Romeo, A.; Berzina, T.; Erokhin, V.; Iannotta, S. A Hybrid Living/Organic Electrochemical Transistor Based on the Physarum Polycephalum Cell Endowed with Both Sensing and Memristive Properties. *Chem. Sci.* **2015**, *6*, 2859−2868.
(63) Nguyen-dang, T.; Chae, S.; Chatsirisupachai, J.; Wakidi, H.; Promarak, V.; Visell, Y.; Nguyen, T. Dual-Mode Organic Electrochemical Transistors Based on Self-Doped Conjugated Polyelectrolytes for Reconfigurable Electronics. *Adv. Mater.* **2022**, *34*, 1−9.
(64) Zeglio, E.; Eriksson, J.; Gabrielsson, R.; Solin, N.; Inganäs, O. Highly Stable Conjugated Polyelectrolytes for Water-Based Hybrid Mode Electrochemical Transistors. *Adv. Mater.* **2017**, *29* (19), 6−11.
(65) Ko, J.; Wu, X.; Surendran, A.; Muhammad, B. T.; Leong, W. L. Self-Healable Organic Electrochemical Transistor with High Transconductance, Fast Response, and Long-Term Stability. *ACS Appl. Mater. Interfaces* **2020**, *12* (30), 33979−33988.
(66) Ikemoto, S. Dopamine Reward Circuitry: Two Projection Systems from the Ventral Midbrain to the Nucleus Accumbens-Olfactory Tubercle Complex. *Brain Res. Rev.* **2007**, *56* (1), 27−78.
(67) Tang, H.; Lin, P.; Chan, H. L. W.; Yan, F. Highly Sensitive Dopamine Biosensors Based on Organic Electrochemical Transistors. *Biosens. Bioelectron.* **2011**, *26* (11), 4559−4563.
(68) Liu, X.; Liu, J. Biosensors and Sensors for Dopamine Detection. *View* **2021**, *2* (1), 1−16.
(69) Alberti, S.; Piccinini, E.; Ramirez, P. G.; Longo, G. S.; Ceolín, M.; Azzaroni, O. Mesoporous Thin Films on Graphene FETs: Nanofiltered. *Amplified and Extended Field-Effect Sensing. Nanoscale* **2021**, *13* (45), 19098−19108.
(70) Liao, C.; Zhang, M.; Niu, L.; Zheng, Z.; Yan, F. Organic Electrochemical Transistors with Graphene-Modified Gate Electrodes for Highly Sensitive and Selective Dopamine Sensors. *J. Mater. Chem. B* **2014**, *2* (2), 191−200.
(71) Stevens, D. L.; Parra, A.; Grunlan, J. C. Thermoelectric Performance Improvement of Polymer Nanocomposites by Selective Thermal Degradation. *ACS Appl. Energy Mater.* **2019**, *2* (8), 5975−5982.
(72) Ishizaki, Y.; Watanabe, A.; Yamamoto, S.; Mitsuishi, M. Controlling Resistive Switching Modes of Ferrocene-Containing Polyelectrolyte Layer-by-Layer Nanofilms. *ACS Appl. Electron. Mater.* **2023**, *5* (7), 3957−3964.

https://doi.org/10.1021/acsaelm.3c01592
ACS Appl. Electron. Mater. 2024, 6, 1211−1222